Biophysical Journal Volume 105 October 2013 1601–1611

Antibody-Induced Acetylcholine Receptor Clusters Inhabit Liquid-Ordered and Liquid-Disordered Domains

Constanza B. Kamerbeek,[†] Virginia Borroni,[†] María F. Pediconi,[†] Satoshi B. Sato,[‡] Toshihide Kobayashi,[‡] and Francisco J. Barrantes[†§*]

[†]Instituto de Investigaciones Bioquímicas de Bahía Blanca, Bahía Blanca, Argentina; [‡]Lipid Biology Laboratory, RIKEN, Saitama, Japan; and [§]Laboratory of Molecular Neurobiology, Institute for Biomedical Research UCA-CONICET, Faculty of Medical Sciences, Catholic University of Argentina, Buenos Aires, Argentina

ABSTRACT The distribution of nicotinic acetylcholine receptor (AChR) clusters at the cell membrane was studied in CHO-K1/A5 cells using fluorescence microscopy. Di-4-ANEPPDHQ, a fluorescent probe that differentiates between liquid-ordered (Lo) and liquid-disordered (Ld) phases in model membranes, was used in combination with monoclonal anti-AChR antibody labeling of live cells, which induces AChR clustering. The so-called generalized polarization (GP) of di-4-ANEPPDHQ was measured in regions of the cell-surface membrane associated with or devoid of antibody-induced AChR clusters, respectively. AChR clusters were almost equally distributed between Lo and Ld domains, independently of receptor surface levels and agonist (carbamoylcholine and nicotine) or antagonist (α-bungarotoxin) binding. Cholesterol depletion diminished the cell membrane mean di-4-ANEPPDHQ GP and the number of AChR clusters associated with Ld membrane domains increased concomitantly. Depolymerization of the filamentous actin cytoskeleton by Latrunculin A had the opposite effect, with more AChR clusters associated with Lo domains. AChR internalized via small vesicles having lower GP and lower cholesterol content than the surface membrane. Upon cholesterol depletion, only 12% of the AChR-containing vesicles costained with the fluorescent cholesterol analog fPEG-cholesterol, i.e., AChR endocytosis was essentially dissociated from that of cholesterol. In conclusion, the distribution of AChR submicron-sized clusters at the cell membrane appears to be regulated by cholesterol content and cytoskeleton integrity.

INTRODUCTION

Nicotinic acetylcholine receptors (AChRs) are members of the Cys-loop family of fast ligand (neurotransmitter)-gated ion channels, all of which are pentameric transmembrane receptor proteins. AChRs are expressed in central and peripheral nervous systems, the neuromuscular junction and the electromotor synapse of electric fish in the latter case. AChR levels and surface organization are determinant for the efficacy of cholinergic synaptic activity. This is evident in the autoimmune disease myasthenia gravis, in which autoantibodies against AChR are present in ~85% of patients (1), inducing the loss of surface AChRs from the neuromuscular junction and resulting in serious impairment of synaptic transmission (2,3). Loss of cell-surface receptors results from an accelerated rate of AChR endocytosis, mimicked in vitro in many cell systems including CHO K1/A5 cells, a Chinese hamster ovary cell line generated in our laboratory (4) that stably expresses adult muscle-type AChR (5–7).

When stained with fluorescent α-bungarotoxin (BTX) and imaged with conventional widefield microscopy, CHO-K1/A5 cells show a finely diffuse fluorescence staining at their surface (5,8). Plasma membrane sheets generated by cell unroofing enabled visualization of AChR puncta as submicron-sized, diffraction-limited spots of ~200 nm (5). Using stimulated emission depletion superresolution microscopy (nanoscopy) and antibody labeling, the diffraction-limited puncta could be resolved into nanoclusters of ~55 nm (9). The organization and amount of these antibody-induced AChR nanoclusters, as well as their interrelationship, were found to be cholesterol (Chol)- and cytoskeleton-dependent (5,9,10). This is remarkably similar to the case of myotubes in culture (11–14), where association of AChR with Chol-rich domains is required for the formation and maintenance of AChR clusters. It was proposed that Chol-rich membrane domains are involved in AChR clustering by promoting local actin cytoskeleton reorganization (15). Chol depletion induces the fragmentation of the relatively large, micron-sized AChR assemblies found in muscle cells (11–14), thus suggesting the existence of conserved mechanisms for maintaining ground levels of surface AChRs (in the absence of nerve or muscle signaling) and their proper supramolecular organization (16).

Segregation of proteins into membrane lipid domains of different biophysical properties has been proposed as a mechanism for the spatiotemporal regulation of signaling and trafficking (17,18). In *Torpedo* electrical organ, AChR arrays are embedded in a lipid microenvironment that differs in physical terms from the rest of the membrane bilayer (19,20). This was also observed in C2C12 myotubes, in which large micron-sized AChR clusters formed upon agrin stimulation resided in more ordered membrane domains (11). However, the effect of this association on AChR endocytic trafficking has not as yet been explored in detail.

To date, Laurdan and di-4-ANEPPDHQ are two of the most commonly used fluorescent probes for studying

Submitted May 29, 2013, and accepted for publication August 21, 2013.

*Correspondence: rtfjb1@yahoo.com

Editor: Amitabha Chattopadhyay.

0006-3495/13/10/1601/11 $2.00

http://dx.doi.org/10.1016/j.bpj.2013.08.039

differences in membrane order in model membranes and living cells. Both probes sense membrane polarity—i.e., the level of water penetration in the membrane—by displaying a blue-shift in their emission spectrum (21,22). The so-called GP—used to calculate the degree of membrane order—is obtained from the differences between the fluorescence emission properties of the dye in liquid-ordered (Lo) and liquid-disordered (Ld) phases (23). It has been demonstrated that the incorporation of proteins into liposomes does not modify the emission spectra of Laurdan or di-4-ANEPPDHQ (21), indicating the suitability of these probes for studying membrane physical properties in living cells. The main advantage of using di-4-ANEPPDHQ instead of Laurdan is that the former is excited in the visible spectrum (488 nm), whereas Laurdan requires excitation in the ultraviolet range of the spectrum (24).

We have previously undertaken combined fluorescence spectroscopy and patch-clamp studies of CHO-K1/A5 cells and surface membranes prepared therefrom using the probe Laurdan (25), enabling the correlation of the temperature-dependent single-channel properties of the AChR with the physical state of the host membrane derived from the temperature-dependence of Laurdan GP. In this work we attempted to obtain spatial information on the relationship between AChR (nano)clusters and the physical state of the host membrane lipid in which the receptors are embedded using di-4-ANEPPDHQ GP. The results obtained highlight the importance of membrane cholesterol and actin cytoskeleton integrity in the maintenance of small AChR nanoclusters. We postulated that such aggregates resemble the organization of supramolecular assemblies of receptors at early embryonic developmental stages (16,26). Furthermore, these aggregates may also bear on the initial phase of antibody-induced clustering in myasthenia.

MATERIAL AND METHODS

Materials

Cholesterol, methyl-β-cyclodextrin (CDx), latrunculin A (Lat A), cytochalasin D (Cyto D), nicotine (Nic), carbamoylcholine chloride (Carb), and dimethyl sulfoxide (DMSO) were purchased from Sigma Chem. Co. (St. Louis, MO). Jasplakinolide (Jaspl) was from Calbiochem (San Diego, CA). BTX, Alexa Fluor^{647}α-bungarotoxin (Alexa^{647}BTX) and Alexa Fluor^{647} antibodies were purchased from Molecular Probes (Eugene, OR) or Invitrogen (Carlsbad, CA). The monoclonal antibody mAb 210 against the main immunogenic region of the AChR α subunit was a gift from Dr. Jon Lindstrom, Univ. of Pennsylvania Med. Center. The fluorescein ester of polyethylene glycol-derivatized cholesterol (fPEG-Chol) was synthesized in Prof. T. Kobayashi and Dr. Satoshi B. Sato's laboratories. Di-4-ANEPPDHQ was a gift from Prof. L. Loew, University of Connecticut Health Center for Cell Analysis & Modeling, Farmington, CT.

Cell culture

CHO-K1/A5 cells were grown in Ham's F12 medium supplemented with 12% fetal bovine serum at 37°C for 2–3 days as previously described (4).

Acute cholesterol depletion/enrichment of cultured cells

CHO-K1/A5 cells were incubated at 37°C for 30 min with different concentrations (5–15 mM) of CDx in medium 1 (M1:140 mM NaCl, 1 mM $CaCl_2$, 1 mM $MgCl_2$, and 5 mM KCl in 20 mM HEPES buffer, pH 7.4) to acutely deplete their cholesterol content before fluorescent labeling as described previously (5). The experiments in Fig. 3 were carried out using a final concentration of 15 mM CDx. For cholesterol enrichment experiments, CDx-Chol complexes were prepared as in Christian et al. (27). Cells were incubated with 15 mM Chol-CDx complexes (CDx/Chol 6:1) at 37°C for 30 min.

Disruption/stabilization of the actin meshwork

CHO-K1/A5 cells were incubated with 4 μM Lat A, 2.5 μM Cyto D, or 1 μM Jaspl at 37°C for 2 h. Stock solutions of these drugs were made in DMSO and working solutions were prepared by diluting the stock in M1. As a control condition, cells were incubated with the maximum volume of DMSO used, always below 0.5% DMSO in M1 (v/v).

AChR internalization triggered by BTX ligation

As described previously by Kumari et al. (7), binding of antibody or BTX triggers the internalization of the AChR. Here, cells were exposed to 500 nM BTX in M1 for 15 min at 4°C. At the end of the incubation period cells were washed thrice with cold M1 and shifted to 37°C for 2 h. In the experiments shown in Fig. 5 (only control BTX internalization) and Fig. 6, Alexa^{647}BTX was used instead of native BTX.

AChR agonist treatment

Cells were incubated with 100 μM Nic and 0.5 mM Carb at 37°C for 30 and 50 min, respectively. Because agonist binding to the receptor is reversible, cells were washed with cold M1 containing the same agonist concentration.

Widefield fluorescence microscopy

CHO-K1/A5 cells were grown on 25 mm diameter glass coverslips in Ham's F12 medium at 37°C and then washed thrice with M1 medium. For surface Chol staining, cells were incubated with 1 μM fPEG-Chol in M1 at 4°C and after washing with M1, observed under the microscope. Cell-surface AChR labeling of CHO-K1/A5 cells was carried out by incubation of cells at 4°C for 1 h with mAb 210 and subsequently with Alexa^{647}-labeled secondary antibody (far red) at 4°C for 1 h, before di-4-ANEPPDHQ treatment in M1 at 4°C for 15 min. Cells were subsequently rinsed thrice with 20 micromolar M1 and mounted for microscope examination. For all experiments a 100× (1.4 N.A.) oil-immersion objective was used for imaging in a Nikon TE-300 inverted microscope. Appropriate dichroic and emission filters were employed to avoid crossover of fluorescence emission. Sixteen bit images were exported for further offline analysis.

Di-4-ANEPPDHQ imaging

After treatment, coverslips were mounted on a slide and immediately transferred to a Nikon TE-300 inverted microscope. Di-4-ANEPPDHQ was excited by a mercury arc; 488 nm light was selected with a Z488/10 band-pass excitation filter (Chroma Technol., Rockingham, VT). Emitted fluorescence was separated from excitation by a dichroic beam splitter (Z488RDC, Chroma) and imaged via a dual-viewer instrument constructed at the Department of NanoBiophotonics, Max Planck Institute for Biophysical Chemistry, Göttingen, Germany. This multichannel imager split

the fluorescence emission into two beams using a second dichroic beam splitter (610 dplc, Chroma). Each beam was then spectrally isolated with bandpass emission filters HQ575/50 and HQ680/50 (Chroma) and imaged onto the two halves of a thermostatically cooled Hamamatsu ORCA-ER C4742-95-12ERG (Hamamatsu Photonics, Hamamatsu City, Japan) charge-coupled device (CCD) camera. To obtain the positionally resolved GP values, fluorescence images were acquired with SlideBook (Intelligent Imaging Innovations, Denver, CO). A quarter-wave plate was placed before the dichroic mirror to reduce polarization-dependent reflectance.

GP of di-4-ANEPPDHQ

The images obtained with the dual-viewer setup required further fine offline alignment. For this purpose, regions of interest (ROIs) of the two simultaneously recorded images were aligned using ad hoc routines in SlideBook and tested for optimization of the two-dimensional alignment by application of Pearson's (28), Manders' (29), and Costes et al. (30) algorithms (see Fig. S1 in the Supporting Material). These algorithms quantify the degree of colocalization of all pixels in the two 256 × 256 images split into the two halves of the CCD camera.

Upon optimization of the colocalization images, the so-called GP of di-4-ANEPPDHQ in the fluorescence images was calculated on a pixel basis from the ratio of fluorescence intensities (I) of the blue-edge channel, with recorded emission wavelengths between 550 and 600 nm (HQ575/50m filter), and the red-edge channel (emission wavelength 655–705 nm, HQ680/50m) based on the following equation:

$$\mathrm{GP} = \frac{I_{550-600} - I_{655-705}}{I_{550-600} + I_{655-705}} \quad (1)$$

GP distributions were obtained from the histograms of the GP images using the software ImageJ (NIH, Bethesda, MD). Background values were set to zero by converting the denominator of the GP function (Eq. 1 above) to a binary image with background values set to zero, nonbackground values set to one, and the binary image multiplied with the GP image as described by Gauss et al. (31).

To validate the experimental system, we prepared giant unilamellar vesicles (GUVs) resembling ordered (DPPC/Chol, 7:3) and disordered (DOPC) phases as in Jin et al. (2006) (Fig. S2). GUVs were imaged with a TCS-SP2 confocal microscope (Leica Mikrosysteme Vertrieb GmbH, Wetzlar, Germany) equipped with an acoustooptical beam splitter. Di-4-ANEPPDHQ emission was collected in the blue-edge and red-edge channels and GP images were generated. As shown in Fig. S2, di-4-ANEPPDHQ successfully differentiates Lo and Ld phases.

When labeled at 4°C with di-4-ANEPPDHQ, the fluorescence signal in live CHO-K1/A5 cells is restricted almost exclusively to the plasma membrane; essentially no internalization of the probe occurs in the time window of 15 min at 4°C (Fig. S3). The corresponding actual excitation and emission spectra of live CHO-K1/A5 cells in suspension as obtained in cuvette experiments is shown in Fig. S4. As expected for a bulk measurement, a single component for di-4-ANEPPDHQ fluorescence emission was observed. The regions of the emitted fluorescence selected by the HQ575/50m (blue-edge) and the HQ680/50m (red-edge) filters are superimposed onto the emission spectrum.

As shown in Fig. S3, fluorescence images of di-4-ANEPPDHQ in a live CHO-K1/A5 cell at the blue-edge (Fig. S3 *A*) and red-edge (Fig. S3 *B*) of the spectrum exhibit different intensities but do not show heterogeneity, even when the two images are superimposed and aligned (Fig. S3 *C*). However, when the spatially resolved GP images were generated, the uneven distribution of the di-4-ANEPPDHQ GP values became apparent (Fig. S3 *D*). Regions of high GP (high order, pseudocolored in *yellow/red*) were particularly noticeable in the thin filopodia and cell-surface protrusions (*arrows* in Fig. S3 *D*). When the areas corresponding to the cell-surface membrane were isolated by masking, mean GP values of control condition cells ranged between 0.36 and 0.48. These figures depended on the experimental conditions (incubation medium, temperature, etc.) before di-4-ANEPPDHQ staining.

Other quantitative image analyses

To measure the spatial relationship between AChR-positive areas with the GP of di-4-ANEPPDHQ in those areas, 32-bit GP images were analyzed with ImageJ after manually outlining ROIs in areas previously aligned with SlideBook software. The average GP of several ROIs was measured within the anti-AChR positive region and in regions of the plasma membrane devoid of anti-AChR label. For illustration purposes, images were processed using ImageJ, scaled with identical parameters, and pseudocolored according to a custom-designed 16-color lookup table.

With the aim of evaluating AChR distribution in relation to membrane mean GP, cells were incubated with the mAb 210 anti-AChR monoclonal antibody followed by Alexa^{647}-labeled secondary antibody. This labeling procedure produces visible AChR clusters in the plasmalemma. After di-4-ANEPPDHQ treatment and imaging, each AChR cluster was manually outlined, selected as a ROI, and analyzed for its GP value with ImageJ. These GP values in AChR clusters were compared with the mean membrane GP and classified into three groups: ROIs with GP values at least 0.001 higher, lower, or equal to those of the mean membrane GP. All experiments were repeated at least three times. In all experiments the number of clusters in each group was normalized on the basis that the total number of clusters in the experiment was equal to 100. Histograms were made by averaging each group of clusters from different experiments, thus reflecting the preference of AChR clusters for a given range of GP values as compared with the average membrane GP for each experimental condition.

RESULTS

GP of di-4-ANEPPDHQ in CHO-K1/A5, a mammalian cell line expressing muscle-type AChR

Di-4-ANEPPDHQ was introduced into the membrane field as an environmentally sensitive styryl fluorescent probe, which differentially senses Ld from Lo phases coexisting in model membranes (32). The probe was subsequently tested in large unilamellar vesicles and neutrophils (33). Here, the probe was first used to label the cell surface of a fibroblast cell line produced in our laboratory, which robustly expresses adult muscle-type AChR at its plasmalemma (4). We employed a dual viewer instrument that allows the simultaneous recording of two spectrally separated signals onto the two halves of the same electron multiplying CCD. In the case of di-4-ANEPPDHQ, this corresponds to a blue-edge channel, reporting indirectly on the Lo regions of the membrane, and a red-edge channel, corresponding to the Ld phase (32,33). Properly aligned (Fig. S1), the two channels should provide an almost perfect two-dimensional map of the spatial distribution of the dye, whose spectral fingerprints report on the microscopic phase state of the membrane.

To evaluate whether di-4-ANEPPDHQ can effectively sense changes in the Chol content of the membrane, cells were treated with CDx, a Chol-depleting agent widely used in cell biology (5,27,34). Previous studies from our

laboratory worked out the optimal concentrations of CDx for achieving acute depletion of cholesterol with minimal affectation of CHO-K1/A5 cell viability or functionality (5). Reduction of the Chol content (Fig. S5) in the membrane in living CHO-K1/A5 cells is associated with a diminution in the mean GP values of di-4-ANEPPDHQ (Fig. 1, *A–C*). This reduction is statistically significant at a CDx concentration of 15 mM (Fig. 1 *C*), when total Chol levels are reduced by at least 50% (34). Interestingly, after CDx treatment the GP images became more homogenous, regions of the membrane with higher GP being more affected by Chol depletion (Fig. 1 *A*). The GP distribution became narrower after CDx treatment, reflecting the loss of compartmentalization in the membrane due to Chol depletion (Fig. 1 *B*).

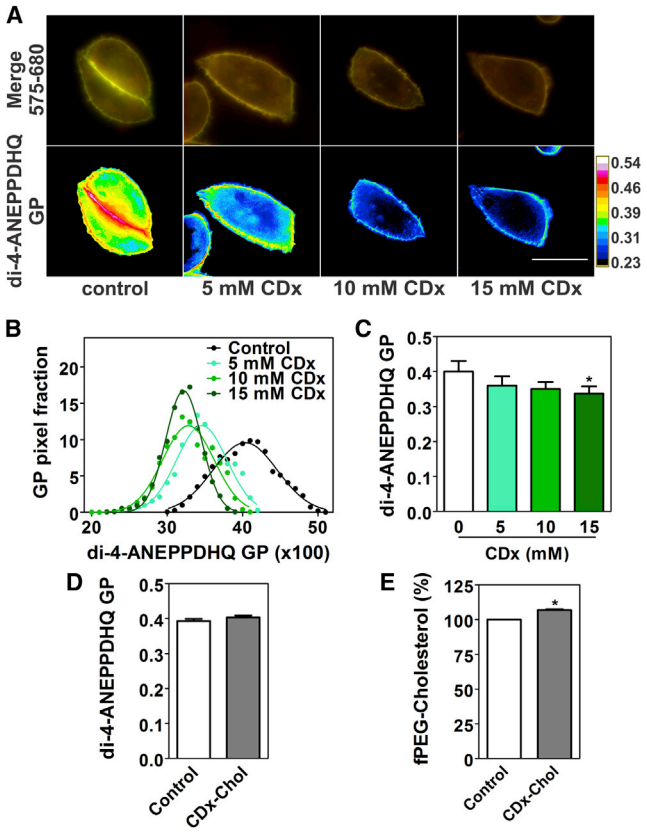

FIGURE 1 Changes in di-4-ANEPPDHQ GP in live AChR-expressing cells induced by cholesterol depletion or enrichment. (*A*) Merged fluorescence images obtained from the blue- and red-edge channels and the corresponding GP images of control and CDx-treated cells. (*B*) Histograms of GP distribution in the plasmalemma of CHO-K1/A5 cells. Distributions on a pixel basis were obtained from GP values of control and CDx-treated cells at the indicated concentrations. GP values were normalized (100 pixels) and their distributions were plotted and fitted to Gaussian functions, corresponding in each case to an individual experiment, thus minimizing the differences in di-4-ANEPPDHQ distribution ($n = 10$ cells for each condition). (*C*) Mean membrane GP values obtained from the Gaussian fits to the pixel-based distributions in (*B*). Graphs show that the mean membrane GP value decreases as a consequence of Chol depletion resulting from CDx treatment, with a statistically significant drop at a concentration of 15 mM CDx. (*D*) Chol enrichment produced by treating cells with CDx-Chol complex before di-4-ANEPPDHQ staining. Mean GP values in the plasmalemma in control and CDx-Chol conditions were not statistically different. (*E*) fPEG-Chol staining shows that a small but statistically significant increase (~10%) in cholesterol takes place at the plasmalemma upon CDx-Chol treatment. Scale bar: 10 μm. (*) $p < 0.05$. To see this figure in color, go online.

In another series of experiments, Chol membrane levels were augmented by incubation of the cells with Chol-CDx complexes (5,27) before staining with di-4-ANEPPDHQ. The probe fPEG-Chol was used to test whether the enrichment in Chol had actually occurred at the plasma membrane (see Fig. 1 *E*). fPEG-Chol is a soluble derivative of Chol that preferentially partitions into Chol-rich membrane domains, thus acting as a Chol sensor in cells (35). A small increase in fPEG-Chol fluorescence (~10%) was observed upon CDx-cholesterol treatment, with no significant difference in di-4-ANEPPDHQ GP values between control and CDx-Chol-treated cells (Fig. 1, *D* and *E*).

Cell surface AChR clusters and membrane lipid composition

In a first series of experiments, CHO-K1/A5 cells were labeled with the anti-AChR monoclonal antibody mAb 210 and Alexa^{647}-labeled secondary antibody; no bleed-through between the Alexa^{647} signal and the two recorded di-4-ANEPPDHQ channels was observed (Fig. S6), thus validating the use of this fluorophore for subsequent experiments. Using this staining protocol, AChR clusters became evident (Fig. 2, *A–C*), allowing us to differentiate between regions in the membrane with (Fig. 2 *D*) or without AChR aggregates (Fig. 2 *E*). Taking advantage of this, we attempted to establish whether there is a correlation between the antibody-induced surface AChR clusters and the physical state of the host membrane. For this purpose, CHO-K1/A5 cells were first labeled with the anti-AChR monoclonal antibody mAb 210 and Alexa^{647}-labeled secondary antibody followed by 20 μM di-4-ANEPPDHQ and imaged. Antibody labeling of AChR at 4°C has no major effects on membrane properties, because the same mean GP value was observed in labeled (Fig. 2 *F*) and unlabeled cells (Fig. 1 *C*). In addition, when the mean GP values obtained from regions of the plasma membrane delimited (Fig. 2 *F*, *mAb 210+*) or not (Fig. 2 *F*, *mAb 210−*) by AChR clusters, they were not found to differ significantly. At first glance this suggests that AChR clusters are associated with domains that are similar in membrane composition, i.e., Chol content, to those in the bulk plasma membrane. However, the lack of difference is most likely because the size of these membrane domains is beyond the resolution of the widefield microscope employed here (9). In the following experiments, each AChR ROI was compared with the mean membrane GP, as described in the Materials and Methods section.

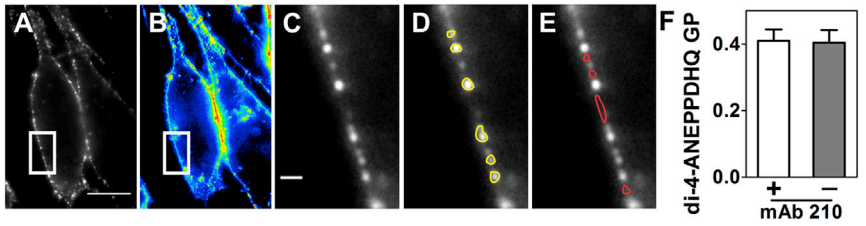

FIGURE 2 GP values in AChR-positive and -negative regions in the plasma membrane. CHO-K1/A5 cells were costained with anti-AChR Alexa^{647} (*A, C, D,* and *E*) and di-4-ANEPPDHQ (*B*). Antibody binding (anti-AChR + Alexa^{647}–conjugated secondary antibody) induces AChR clustering, making clearly apparent AChR-rich spots and areas devoid of AChR (*A*). Upon alignment of the selected regions (example highlighted by the *white rectangle*) algorithms were applied to quantify the degree of colocalization. (*B*) Corresponding di-4-ANEPPDHQ GP image. (*C–E*) Magnified membrane area. Notice the clear antibody-positive spots, identified in *D* as AChR clusters (positive mAb 210 ROIs, *yellow*) and AChR-negative (*mAb 210−*) membrane areas (*E*), outlined in red. (*F*) Mean GP values obtained from plasma membrane mAb 210+ or mAb 210− ROIs, respectively. Scale bar: 10 μm in (*A* and *B*) and 1 μm in (*C*, *D*, and *E*). ($n = 3$). To see this figure in color, go online.

Distribution of AChR clusters in membrane domains depends on Chol and the integrity of the cytoskeleton

One of the possible interpretations of the previous results is that under control conditions surface AChR clusters do not show a preference for any specific membrane domain. Chol is one of the main structural components of lipid ordered domains in the membrane (33) and is an important factor in stabilizing AChR and determining the mechanism and rate of AChR endocytosis (34). To evaluate whether Chol affects the association of AChR with membrane domains, Chol was depleted by treating cells with 15 mM CDx at 37°C for 30 min. At the end of the incubation cells were stained as in Fig. 2 with anti-AChR-Alexa^{647} and di-4-ANEPPDHQ at 4°C. Images were processed as described in Materials and Methods to obtain the distribution of AChR clusters with respect to the mean GP of the membrane. As previously reported (5), CDx treatment reduced the number of AChR clusters at the membrane and the mean membrane GP (Fig. 3, *A* and *B*). Almost 90% of AChR clusters in Chol-depleted cells were localized in membrane domains with GP values lower than those found under control conditions (Fig. 3 *C*). More importantly, Chol depletion also increased the number of AChR clusters associated with GP values lower than the mean membrane GP, with a concomitant decrease in clusters associated with higher membrane GP values (Fig. 3 *D*).

In CHO-K1/A5 cells, binding of the antagonist BTX or anti-AChR antibodies results in AChR internalization that occurs independently of clathrin, caveolin, or dynamin, but requires actin polymerization (7). In contrast, in Chol-depleted cells AChR internalization proceeds by a ligand-, clathrin-, and dynamin-independent pathway that is not affected by disruption of the actin cytoskeleton (34). These differences led us to investigate whether AChR localization in plasma membrane regions with different GP values depends on cytoskeletal integrity. Cyto D was previously shown to decrease the number of actin stress fibers, which clumped together; Jaspl induced polymerization of monomeric actin into amorphous masses and Lat A triggered a massive disruption of the stress fibers (34). CHO-K1/A5 cells also changed their morphology as a consequence of actin cytoskeleton disruption; this change is indicative of the efficacy of the treatment (see (34) and Fig. S7). Moreover, as previously reported (7), disruption of the actin cytoskeleton by Cyto D inhibits AChR internalization triggered by the antagonist BTX. This was also observed upon incubation of CHO-K1/A5 cells with Lat A (Fig. 4, BTX *internalization*).

Applying the same analysis as in Fig. 3, disruption of the actin cytoskeleton by Lat A increased the number of AChR clusters with a mean GP value higher than the mean membrane GP, with a concomitant decrease in AChR clusters associated with low GP domains (Fig. 4, *A* and *B*). A similar tendency was observed with Cyto D and Jaspl treatments, although the dispersion of the data precluded any statistically significant conclusions (Fig. 4). Changes in the mean GP value of the plasma membrane were not detected by incubation with any of the three drugs (Fig. 4 *C*). Cytoskeletal disruption produced by Lat A-induced actin depolymerization leads to the redistribution of AChR (nano)clusters in a manner opposite to that observed with Chol depletion (Fig. 3).

Association of surface and internalized AChR with lipid domains

Binding of the antagonist BTX induces AChR internalization with a time constant of 1.98 h (5,7). We then evaluated the localization of the AChR clusters remaining at the cell surface after ligand-induced endocytosis associated with lipid domains having different GP values. Cells were treated with cold BTX, incubated at 37°C for 2 h to allow for AChR internalization, and finally stained with the monoclonal antibody mAb 210/ Alexa^{647}-labeled secondary antibody and di-4-ANEPPDHQ (Fig. 5 *A*). The internalization triggered by BTX did not modify the distribution in lipid domains of those AChRs remaining at the cell surface (Fig. 5 *B*). Similarly, no modifications in the mean GP of the plasmalemma were detected upon BTX binding and subsequent AChR internalization (Fig. 5 *C*). Therefore, neither antagonist binding nor an endocytosis-mediated decrease in the

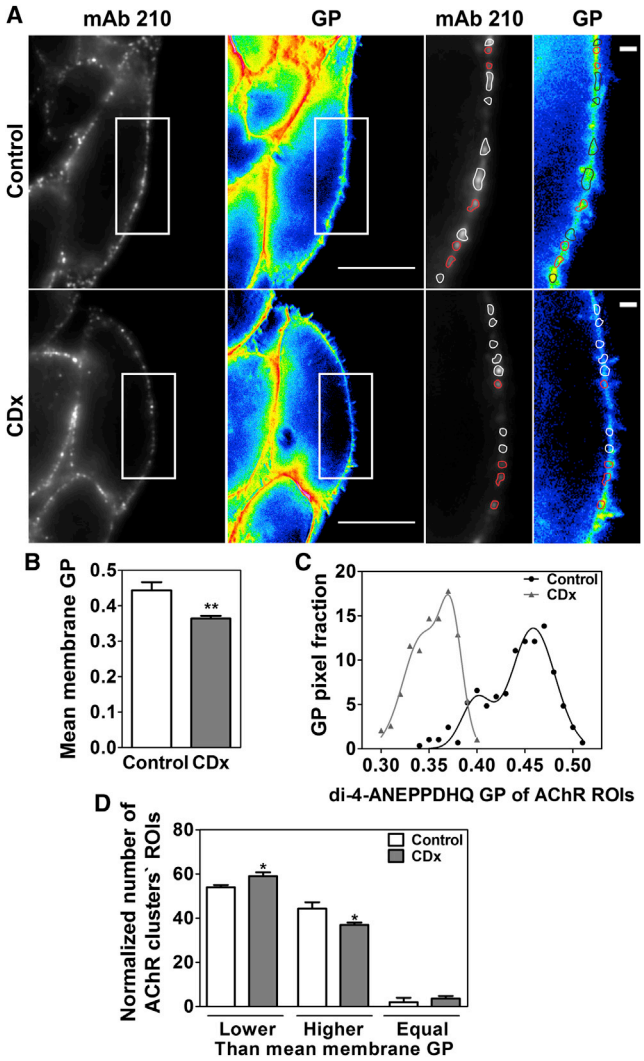

FIGURE 3 AChR distribution in areas with different GP values is affected by Chol depletion. (*A*) CHO-K1/A5 cells costained with anti-AChR Alexa^{647} (*mAb 210*) and di-4-ANEPPDHQ as in Fig. 2 (*control versus Chol depletion*). Regions of the cell-surface membrane on which the analysis was carried out are highlighted with a white rectangle. AChR clusters associated with areas having GP values lower than the mean GP of the cell membrane are outlined in white; AChR clusters with higher-than-the-mean GP are outlined in red. (*B*) As expected, CDx treatment also reduced mean membrane GP, as a result of Chol depletion. (*C*) Histograms of GP values obtained from the underlying plasmalemma of AChR clusters and fitted as the sum of two Gaussian functions. (*D*) AChR clusters with mean GP lower, higher, or equal to the mean membrane GP. An increase in AChR clusters associated with regions having mean GP lower than the membrane resulted from CDx treatment. Scale bar in (*A*): 10 μm in images with a white rectangle, and 1 μm in magnified images. (*) $p < 0.05$, (**) $p < 0.01$. ($n = 3$). To see this figure in color, go online.

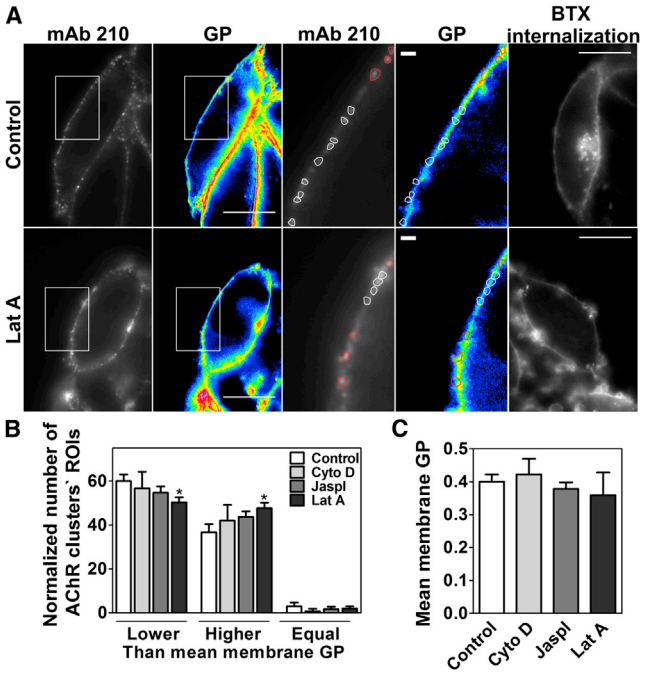

FIGURE 4 Actin cytoskeleton integrity affects the distribution of the AChR in areas with different GP values. Cells were incubated at 37°C for 2 h with Cyto D, Jaspl, and Lat A, three drugs that affect the actin cytoskeleton, and dimethyl sulphoxide as control. (*A*) Control and Lat A-treated cells, stained and analyzed as in Fig. 3 *A*. BTX internalization: Cells were stained with Alexa^{647}BTX and then incubated at 37°C for 2 h. As shown in the image, Lat A treatment inhibits AChR internalization. (*B*) Statistically significant differences in the distribution of AChR were observed upon Lat A treatment. (*C*) The drugs used to alter the integrity of the actin cytoskeleton did not affect the mean GP of the membrane. Scale bar in (*A*): 10 μm in images with a white rectangle and BTX internalization images, and 1 μm in magnified images. (*) $p < 0.05$. ($n = 3$). To see this figure in color, go online.

number of surface AChRs affects receptor distribution in membrane domains with different GP values.

The possible effects of agonist binding were then investigated. Continued exposure to a high concentration of agonist leads to AChR desensitization. CHO-K1/A5 cells were incubated with the agonists Nic and Carb for 30 and 50 min, respectively, before antibody and di-4-ANEPPDHQ staining as in Fig. 2. As shown in Fig. 5, after agonist-induced receptor desensitization, no changes in the mean GP value of the plasmalemma (Fig. 5 *C*) or the AChR distribution in membrane domains could be observed (Fig. 5 *B*).

Results on AChR cluster distribution shown in Figs. 3, 4, and 5, are summarized in Table 1.

We next evaluated the fate of internalized AChR and its association with intracellular membrane compartments. Cells were labeled with di-4-ANEPPDHQ at 4°C, followed by incubation at 37°C for 2 h to allow receptor internalization. At the end of the incubation, di-4-ANEPPDHQ was found in small vesicles and in an internal central compartment (Fig. 6 *A*, di-4-ANEPPDHQ, *arrow and arrowhead*, respectively). The vesicles emitted predominantly at the red-edge channel (Fig. 6 *A*, 575 nm/680 nm, *arrow*), whereas di-4-ANEPPDHQ present in the central compartment emitted predominantly at the blue-edge channel (Fig. 6 *A*, 575 nm/680 nm, *arrowhead*). As a consequence, the vesicles had low GP and the central compartment had

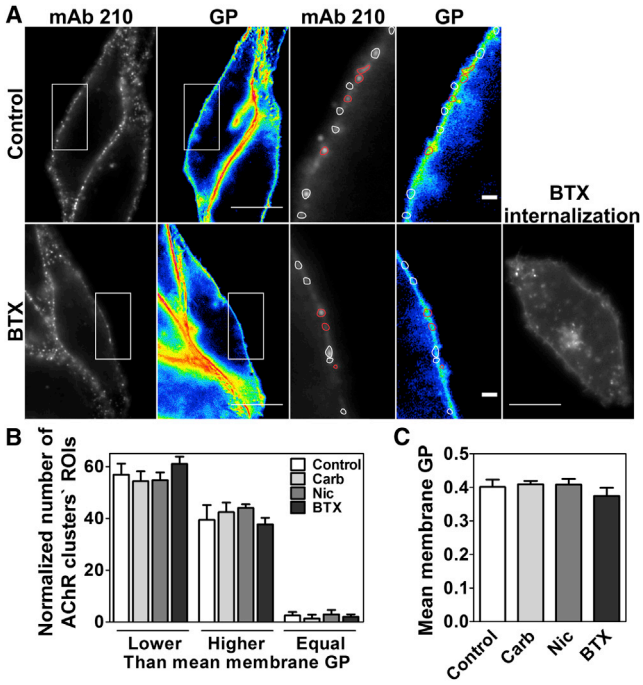

FIGURE 5 Neither AChR internalization induced by BTX nor agonist treatment affects AChR distribution between high and low GP regions. (*A*) Incubation with and without BTX was carried out at 37°C for 2 h. Staining conditions and image analysis were done as in Fig. 3 *A*. To verify that AChR internalization actually occurred within the incubation interval, an additional control was carried out by staining the cells with Alexa^{647}BTX during the incubation period (BTX *internalization*). (*B*) Distribution of AChR in areas of di-4-ANEPPDHQ GP higher, lower, or equal to the mean GP values upon receptor internalization or agonist treatment (Nic and Carb). No statistically significant differences were observed. (*C*) Incubation with BTX, Carb, or Nic did not modify mean GP values of the membrane. Scale bar: 10 μm (images with *white rectangle*); 1 μm (*magnified images*). ($n = 3$). To see this figure in color, go online.

high GP (Fig. 6 *A*, GP, *black arrow and arrowhead*, respectively). This difference in the order of the membranes may reflect differences in the Chol content of these compartments. To test this, cells were incubated at 37°C for 2 h with the fluorescent Chol probe fPEG-Chol. Because di-4-ANEPPDHQ and fPEG-Chol costaining would cause spectral bleed-through, experiments could not be undertaken with the two probes simultaneously. fPEG-Chol bound to plasma membrane is slowly internalized into endosomes together with lipid raft markers via a clathrin-independent pathway (7,35). As shown in Fig. 6 *A*, after 2 h at 37°C fPEG-Chol is present in the plasma membrane and in an internal compartment (*arrowhead*), with morphology similar to that of the di-4-ANEPPDHQ-containing compartment, suggesting that the higher GP of this compartment is related to higher Chol content. Thus, as in the plasmalemma, di-4-ANEPPDHQ GP appears to be a reliable probe of biophysical properties of membrane compartments and mirrors their Chol content.

A staining protocol was then devised to visualize exclusively the fluorescent-labeled AChR and di-4-ANEPPDHQ present in the membrane at the beginning of the experiment. For this purpose cells were incubated with Alexa^{647}BTX and di-4-ANEPPDHQ at 4°C, followed by incubation at 37°C for 2 h to allow internalization of both probes. This staining protocol enabled the visualization of internalized AChR in BTX-labeled individual vesicles (Fig. 6 *B*, BTX, *arrow*), 40% of which also exhibited di-4-ANEPPDHQ staining (Fig. 6 *B*, 680 nm/BTX and 575 nm/BTX, respectively, *arrow*). These vesicles had mean GP values lower than that of the plasma membrane (Fig. 6 *C*). Moreover, internalized AChR vesicles did not colocalize with fPEG-Chol, thus confirming that the lower GP of AChR-containing vesicles reflected their lower Chol content (Fig. 6 *D*, *arrow*).

TABLE 1 Modifications produced in CHO-K1/A5 cells after treatment with different drugs

	Mean membrane GP vs. control condition			Predominant location of AChR clusters vs. control condition		
Drug treatment	Lower GP	Higher GP	Without change	Lower GP	Higher GP	Without change
CDx	X			X		
Cyto D			X			X
Jaspl			X			X
Lat A			X		X	
BTX			X			X
Nic			X			X
Carb			X			X

CDx treatment accelerates AChR endocytosis (34) and changes the distribution of surface AChR in cell-surface domains (Fig. 3). To test whether these changes were also present in internalized AChR, cells were incubated with BTX and fPEG-Chol and shifted to 37°C for 30 min in the presence or absence of CDx. In control cells, fluorescent BTX and fPEG-Chol were poorly internalized (Fig. 6 *E*, BTX and fPEG-Chol, *control*). In contrast, in CDx-treated cells AChR was internalized in small vesicles, only 12% of which colocalized with fPEG-Chol (Fig. 6 *E*, BTX, *CDx*). Moreover, total fPEG-Chol content was reduced and most of the label was present in vesicles inside the cell (Fig. 6 *E*, fPEG-Chol, *CDx*). These results suggest that AChR is internalized in endosomes with low Chol levels, independently of the endocytic entry route.

DISCUSSION

Cell membranes have lateral heterogeneities or lipid domains that may act as organizing centers for signaling, providing the requisite concentration of molecules for efficient signal transduction. The main characteristic of these heterogeneities is that their lipids are in a more ordered phase than the bulk lipids of the membrane. The possibility of assembling/disassembling these domains adds to the spatiotemporal control over the signaling processes (36,37).

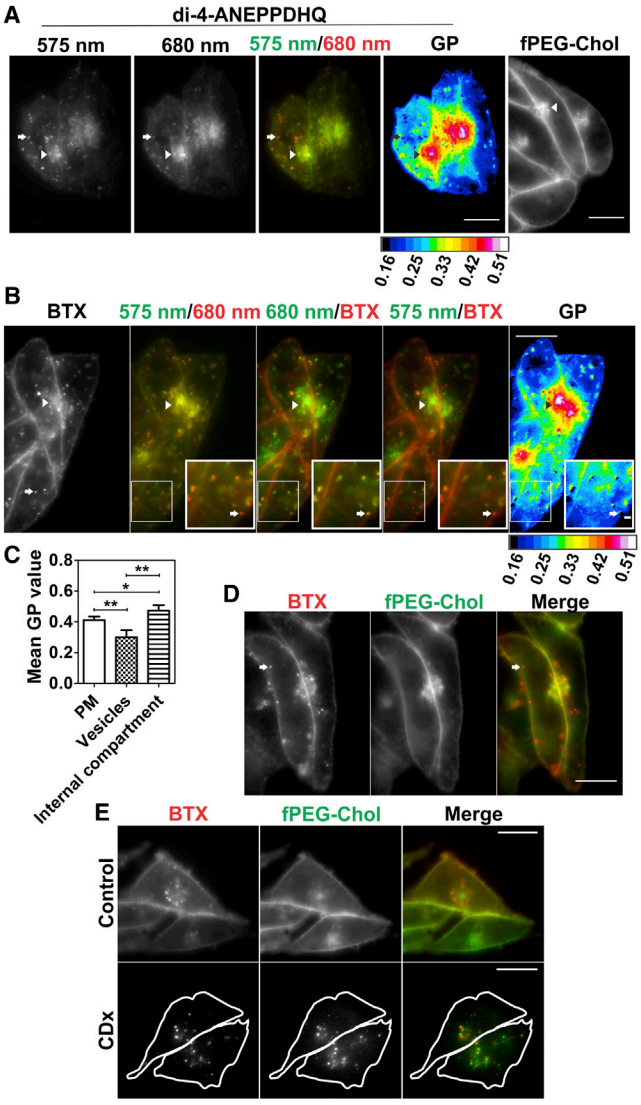

FIGURE 6 Di-4-ANEPPDHQ, fPEG-Chol, and AChR internalization and their intracellular distribution. (*A*) CHO-K1/A5 cells were incubated with di-4-ANEPPDHQ or fPEG-Chol at 4°C and shifted to 37°C for 2 h. Di-4-ANEPPDHQ intracellular localization could be seen in a central compartment (di-4-ANEPPDHQ, *arrowhead*) or in vesicles (di-4-ANEPPDHQ, *arrow*). Corresponding GP image of the cells treated as above. fPEG-Chol was internalized to a central compartment as with di-4-ANEPPDHQ (*arrowhead*). Cells were stained with di-4-ANEPPDHQ and Alexa^{647}BTX (*B*) or fPEG-Chol and Alexa^{647}BTX (*D*) at 4°C and shifted to 37°C for 2 h. Some AChR vesicles colocalized with the red-edge channel signal of di-4-ANEPPDHQ but not with the blue-edge signal (*B*, 680 nm/BTX and 575 nm/BTX, respectively, *arrow*). (*C*) Mean GP value calculated in AChR vesicles and in the internal compartment compared with plasma membrane (PM) mean GP. (*D*) AChR vesicles did not colocalize with fPEG-Chol (*arrow*), but the internal compartment did colocalize. (*E*) BTX and fPEG-Chol internalization was evaluated in the presence or absence of CDx at 37°C for 30 min. In the control condition a similar pattern of internalization was observed for both probes at 30 min or 2 h (*control* and Fig. 6 *A*, *fPEG-Chol*, respectively). In CDx-treated cells, BTX and fPEG-Chol were internalized exclusively in vesicles. Colocalization amounted to ~12%. Scale bar in (*A, C,* and *E*): 10 μm, and 1 μm in magnified images. (*) $p < 0.05$, (**) $p < 0.01$. ($n = 3$). To see this figure in color, go online.

Cholesterol is one of the most abundant components of the lateral heterogeneities of cell membranes in general and of the postsynaptic membrane of cholinergic synapses in particular, where it modulates some functional properties and distribution of the AChR protein (16,26,38). The mechanisms by which cholesterol-AChR interactions are finally translated into the observed changes in the receptor's ligand binding affinity, ion channel properties, or distribution are still not fully understood (16,18,19,38). The main thrust of this work was to establish whether there is a correlation between the state of association (clustering) of the AChR protein and the physical state of Chol-related membrane domains at the cell membrane. For this purpose, use was made of di-4-ANEPPDHQ, an environmentally sensitive styryl fluorescent probe, which reports on the relative proportion of Lo and Ld domains coexisting in model membranes regardless of domain size (32). The fluorescence emission spectrum of di-4-ANEPPDHQ has been reported to be blue-shifted by ~60 nm in Lo phases with respect to Ld phases (32). This property was advantageously exploited to determine the phase (and indirectly the Chol content) of the plasma membrane associated with AChR clusters. Because GP values are intensity ratios, the measurements are independent of local probe concentration or surface area (39). The use of fluorescence microscopy with a dual viewer system provided spatial resolution and circumvented the distortion of measurements occurring with sequential imaging caused by the delay in image acquisition. The degree of order of the cell-surface membrane observed in CHO K1/A5 cells using di-4-ANEPPDHQ was similar to that measured by fluorescence spectroscopy of isolated CHO-K1/A5 membranes using the probe Laurdan (25). In this study we were able not only to quantify but also to spatially resolve the GP of the AChR-associated membrane (Fig. 2).

Membrane GP was sensitive to the Chol content of the membrane, regions of high GP being most affected by changes in Chol levels (Fig. 1 *A*). This was expected, as regions of high GP correspond to more ordered membrane domains, with higher Chol content (33). Removing Chol led to changes in GP distribution: the curve was shifted to the left, became narrower, and could be fitted more accurately with a single Gaussian function (Fig. 1 *B*). The mean GP of the membrane decreased, demonstrating that on a pixel basis di-4-ANEPPDHQ GP imaging provides a good estimate of Chol content (23,32,33).

AChR is present at the plasma membrane of CHO-K1/A5 cells in the form of clusters of ~55 nm only resolved by superresolution microscopy (9,10). Under control conditions at 4°C and in the absence of any external influence the mean GP of the membrane associated with AChR clusters did not differ from the mean GP of the membrane without AChR clusters. This lack of preference was previously observed with AChR reconstituted in model membrane systems (40) and in resting C2C12 cells using

Laurdan GP (11). In C2C12 cells, AChR has been reported to associate with more ordered lipid domains upon agrin treatment, which triggers the formation of AChR micron-sized clusters, the stability of these clusters also being dependent on the association of the AChR with Chol-rich domains (11,41). Association of AChR with domains of high lipid order would be subject to regulation by specific signals. In this regard, AChR organization at the membrane in CHO-K1/A5 cells does not progress as far as in C2C12 cells because of the lack of muscle-specific signaling/clustering proteins like Musk and rapsyn (5,11). Chol acts as a stabilizing factor for the AChR in the membrane (18,26) and its depletion accelerates AChR endocytosis, rerouting the endocytic trail to an Arf6-dependent pathway (34). Modification of the AChR stability and route may be the consequence of altered Chol content in lipid domains associated with AChR clusters in the membrane. Indeed, when cells were Chol-depleted, the distribution of AChR clusters was altered; AChR clusters associated preferentially with low GP domains (Fig. 3). These experiments were carried out after CDx treatment, when half the AChR were already internalized, thus affecting the population of AChRs remaining at the cell surface. Interestingly, AChR is internalized in vesicles that do not colocalize with the fluorescent Chol analog fPEG-Chol and have lower GP than the plasma membrane (Fig. 6). This is independent of the endocytic route followed by the AChR, because the same phenomenon is observed in Chol-depleted cells, where AChR follows a different endocytic pathway (34).

In another series of experiments the Chol content of the intracellular compartments was probed with fPEG-Chol under conditions in which only the plasma membrane was labeled (see Material and Methods), thus measuring internalized Chol arising exclusively from the cell surface membrane. The results suggest that the association of AChR with domains of lower GP (i.e., lower Chol content) favors endocytosis. Given the weight of evidence in support of the role of Chol as an AChR stabilizing factor (16,18,26), the possibility that AChR clusters remaining at the surface are associated with domains with lower GP is less likely.

As with other proteins (42,43), distribution of surface AChR clusters in lipid domains is independent of AChR surface levels. When cells are labeled with BTX and 50% of AChR is internalized, the distribution of AChR in lipid domains is similar to that in cells where AChR is not internalized (Fig. 5). This suggests that AChR molecules contribute to the organization of the lipids that surround them, a contention that has been developed on the basis of considerable experimental evidence accumulated in the course of the last two decades (19,26).

Other factors like Chol availability or association with the cytoskeleton are required for organization of the AChR lipid environment. Actin disruption modifies the distribution of AChR clusters in lipid domains. Treatment with Lat A, a drug that binds to actin monomers and prevents their incorporation into new filaments (44,45), results in the association of the AChR with domains with higher GP (Fig. 4). This implies that the distribution of surface AChR in lipid domains is indeed regulated by the actin cytoskeleton. Other signaling proteins like G-protein coupled receptors (46,47), ERK (48), and Src families kinases (49) show a similar regulation by actin and it was proposed that association/dissociation with ordered lipid domains serves to control the transduction of the signal. Modifications in AChR cluster distribution by actin cytoskeleton disruption could be the consequence of alterations in the structure of lipid domains and/or impaired interactions between actin cytoskeleton and the AChR. Actin cytoskeleton has been observed to impart order to membrane lipids (50,51) and it was proposed that actin may function as a structuring factor of lipid domains in cells (52). However, we detected no difference in the mean GP of the plasma membrane after actin disruption with any of the drugs tested (Fig. 4 *C*). Thus, in our system actin disruption does not appear to induce a global change in the fluidity of the membrane, suggesting that the structure of the lipid domains is conserved. Interestingly, AChR internalization induced by ligand binding is inhibited by disruption of the actin cytoskeleton (see (7) and Fig. 4). The role of actin cytoskeleton and its dynamic on AChR stability is complex and far from clear. Ligand-induced AChR internalization requires actin polymerization (7), but interaction with actin is necessary to form, stabilize, and maintain a high order AChR aggregates found in muscle cells in cultures like C2C12 cells (11,53,54).

One take-home lesson from the present results is that actin cytoskeleton stability is related to AChR organization at the cell surface. Upon agrin signaling, the structuring effect of actin on ordered lipid domains allows AChR clusters associated with these domains to coalesce, associate with clustering proteins, and form the micron-sized aggregates found in C2C12 muscle cells (11,15). In CHO-K1/A5 cells, coupling of AChR nanoclusters and actin polymerization facilitates AChR internalization (7). If the intact actin cytoskeleton prevents the association of small AChR clusters with domains with high GP, it may be assumed that its disruption will remove this barrier (Fig. 4), the ensuing association being accompanied by an increase in the size of AChR nanoclusters (10) and a reduction in the AChR internalization rate (7).

SUPPORTING MATERIAL

Seven figures are available at http://www.biophysj.org/biophysj/supplemental/S0006-3495(13)00986-7.

We thank Prof. L. Loew for a sample of di-4-ANEPPDHQ and to Dr. Silvia Antollini and Vanesa Perillo for help in the preparation of GUVs.

This work was supported by grants PIP No. N° 112-201101-01023 from the Scientific Research Council of Argentina (CONICET), PICT 0559, 1003, and 2011-0604 from the National Agency for Scientific Res., FONCyT, of the Ministry of Science and Technology of Argentina to F.J.B.

REFERENCES

1. Lindstrom, J. M., M. E. Seybold, …, D. D. Duane. 1998. Antibody to acetylcholine receptor in myasthenia gravis: prevalence, clinical correlates, and diagnostic value. 1975. *Neurology.* 51:933–938.
2. Drachman, D. B. 1994. Myasthenia gravis. *N. Engl. J. Med.* 330:1797–1810.
3. Gomez, A. M., J. Van Den Broeck, …, M. Losen. 2010. Antibody effector mechanisms in myasthenia gravis-pathogenesis at the neuromuscular junction. *Autoimmunity.* 43:353–370.
4. Roccamo, A. M., M. F. Pediconi, …, F. J. Barrantes. 1999. Cells defective in sphingolipids biosynthesis express low amounts of muscle nicotinic acetylcholine receptor. *Eur. J. Neurosci.* 11:1615–1623.
5. Borroni, V., C. J. Baier, …, F. J. Barrantes. 2007. Cholesterol depletion activates rapid internalization of submicron-sized acetylcholine receptor domains at the cell membrane. *Mol. Membr. Biol.* 24:1–15.
6. Higgins, L. S., and D. K. Berg. 1988. Metabolic stability and antigenic modulation of nicotinic acetylcholine receptors on bovine adrenal chromaffin cells. *J. Cell Biol.* 107:1147–1156.
7. Kumari, S., V. Borroni, …, F. J. Barrantes. 2008. Nicotinic acetylcholine receptor is internalized via a Rac-dependent, dynamin-independent endocytic pathway. *J. Cell Biol.* 181:1179–1193.
8. Gallegos, C. E., M. F. Pediconi, and F. J. Barrantes. 2008. Ceramides modulate cell-surface acetylcholine receptor levels. *Biochim. Biophys. Acta.* 1778:917–930.
9. Kellner, R. R., C. J. Baier, …, F. J. Barrantes. 2007. Nanoscale organization of nicotinic acetylcholine receptors revealed by stimulated emission depletion microscopy. *Neuroscience.* 144:135–143.
10. Wenz, J. J., V. Borroni, and F. J. Barrantes. 2010. Statistical analysis of high-resolution light microscope images reveals effects of cytoskeleton-disrupting drugs on the membrane organization of the nicotinic acetylcholine receptor. *J. Membr. Biol.* 235:163–175.
11. Stetzkowski-Marden, F., K. Gaus, …, J. Cartaud. 2006. Agrin elicits membrane lipid condensation at sites of acetylcholine receptor clusters in C2C12 myotubes. *J. Lipid Res.* 47:2121–2133.
12. Stetzkowski-Marden, F., M. Recouvreur, …, J. Cartaud. 2006. Rafts are required for acetylcholine receptor clustering. *J. Mol. Neurosci.* 30:37–38.
13. Willmann, R., S. Pun, …, C. Fuhrer. 2006. Cholesterol and lipid microdomains stabilize the postsynapse at the neuromuscular junction. *EMBO J.* 25:4050–4060.
14. Zhu, D., W. C. Xiong, and L. Mei. 2006. Lipid rafts serve as a signaling platform for nicotinic acetylcholine receptor clustering. *J. Neurosci.* 26:4841–4851.
15. Cartaud, A., F. Stetzkowski-Marden, …, J. Cartaud. 2011. Agrin triggers the clustering of raft-associated acetylcholine receptors through actin cytoskeleton reorganization. *Biol. Cell.* 103:287–301.
16. Barrantes, F. J. 2010. Cholesterol effects on nicotinic acetylcholine receptor: cellular aspects. *Subcell. Biochem.* 51:467–487.
17. Allen, J. A., R. A. Halverson-Tamboli, and M. M. Rasenick. 2007. Lipid raft microdomains and neurotransmitter signalling. *Nat. Rev. Neurosci.* 8:128–140.
18. Barrantes, F. J. 2007. Cholesterol effects on nicotinic acetylcholine receptor. *J. Neurochem.* 103 (*Suppl 1*):72–80.
19. Barrantes, F. J. 2004. Structural basis for lipid modulation of nicotinic acetylcholine receptor function. *Brain Res. Brain Res. Rev.* 47:71–95.
20. Jones, O. T., and M. G. McNamee. 1988. Annular and nonannular binding sites for cholesterol associated with the nicotinic acetylcholine receptor. *Biochemistry.* 27:2364–2374.
21. Dinic, J., H. Biverståhl, …, I. Parmryd. 2011. Laurdan and di-4-ANEPPDHQ do not respond to membrane-inserted peptides and are good probes for lipid packing. *Biochim. Biophys. Acta.* 1808:298–306.
22. Parasassi, T., M. Di Stefano, …, E. Gratton. 1994. Cholesterol modifies water concentration and dynamics in phospholipid bilayers: a fluorescence study using Laurdan probe. *Biophys. J.* 66:763–768.
23. Miguel, L., D. M. Owen, …, E. C. Jury. 2011. Primary human CD4+ T cells have diverse levels of membrane lipid order that correlate with their function. *J. Immunol.* 186:3505–3516.
24. Owen, D. M., C. Rentero, …, K. Gaus. 2012. Quantitative imaging of membrane lipid order in cells and organisms. *Nat. Protoc.* 7:24–35.
25. Zanello, L. P., E. Aztiria, …, F. J. Barrantes. 1996. Nicotinic acetylcholine receptor channels are influenced by the physical state of their membrane environment. *Biophys. J.* 70:2155–2164.
26. Barrantes, F. J. 2012. Regulation of the nicotinic acetylcholine receptor by cholesterol as a boundary lipid. *In* Cholesterol Regulation of Ion Channels and Receptors. I. Levitan and F. J. Barrantes, editors. John Wiley & Sons, Hoboken, NJ, pp. 183–204.
27. Christian, A. E., M. P. Haynes, …, G. H. Rothblat. 1997. Use of cyclodextrins for manipulating cellular cholesterol content. *J. Lipid Res.* 38:2264–2272.
28. Manders, E. M., J. Stap, …, J. A. Aten. 1992. Dynamics of three-dimensional replication patterns during the S-phase, analyzed by double labelling of DNA and confocal microscopy. *J. Cell Sci.* 103:857–862.
29. Manders, E. M., F. J. Verbeek, and J. A. Aten. 1993. Measurement of co-localization of objects in dual-colour confocal images. *J. Microsc.* 169:375–382.
30. Costes, S. V., D. Daelemans, …, S. Lockett. 2004. Automatic and quantitative measurement of protein-protein colocalization in live cells. *Biophys. J.* 86:3993–4003.
31. Gaus, K., S. Le Lay, …, M. A. Schwartz. 2006. Integrin-mediated adhesion regulates membrane order. *J. Cell Biol.* 174:725–734.
32. Jin, L., A. C. Millard, …, L. M. Loew. 2005. Cholesterol-enriched lipid domains can be visualized by di-4-ANEPPDHQ with linear and nonlinear optics. *Biophys. J.* 89:L04–L06.
33. Jin, L., A. C. Millard, …, L. M. Loew. 2006. Characterization and application of a new optical probe for membrane lipid domains. *Biophys. J.* 90:2563–2575.
34. Borroni, V., and F. J. Barrantes. 2011. Cholesterol modulates the rate and mechanism of acetylcholine receptor internalization. *J. Biol. Chem.* 286:17122–17132.
35. Sato, S. B., K. Ishii, …, T. Kobayashi. 2004. Distribution and transport of cholesterol-rich membrane domains monitored by a membrane-impermeant fluorescent polyethylene glycol-derivatized cholesterol. *J. Biol. Chem.* 279:23790–23796.
36. Coskun, U., and K. Simons. 2010. Membrane rafting: from apical sorting to phase segregation. *FEBS Lett.* 584:1685–1693.
37. Scott, J. L., C. A. Musselman, …, R. V. Stahelin. 2012. Emerging methodologies to investigate lipid-protein interactions. *Integr. Biol. (Camb).* 4:247–258.
38. Barrantes, F. J., V. Bermudez, …, C. Kamerbeek. 2010. Boundary lipids in the nicotinic acetylcholine receptor microenvironment. *J. Mol. Neurosci.* 40:87–90.
39. Gaus, K., T. Zech, and T. Harder. 2006. Visualizing membrane microdomains by Laurdan 2-photon microscopy. *Mol. Membr. Biol.* 23:41–48.
40. Bermúdez, V., S. S. Antollini, …, F. J. Barrantes. 2010. Partition profile of the nicotinic acetylcholine receptor in lipid domains upon reconstitution. *J. Lipid Res.* 51:2629–2641.
41. Campagna, J. A., and J. Fallon. 2006. Lipid rafts are involved in C95 (4,8) agrin fragment-induced acetylcholine receptor clustering. *Neuroscience.* 138:123–132.
42. Plowman, S. J., C. Muncke, …, J. F. Hancock. 2005. H-ras, K-ras, and inner plasma membrane raft proteins operate in nanoclusters with differential dependence on the actin cytoskeleton. *Proc. Natl. Acad. Sci. USA.* 102:15500–15505.
43. Tian, T., A. Harding, …, J. F. Hancock. 2007. Plasma membrane nanoswitches generate high-fidelity Ras signal transduction. *Nat. Cell Biol.* 9:905–914.

44. Spector, I., N. R. Shochet, …, A. Groweiss. 1983. Latrunculins: novel marine toxins that disrupt microfilament organization in cultured cells. *Science.* 219:493–495.

45. Yarmola, E. G., T. Somasundaram, …, M. R. Bubb. 2000. Actin-latrunculin A structure and function. Differential modulation of actin-binding protein function by latrunculin A. *J. Biol. Chem.* 275:28120–28127.

46. Ganguly, S., and A. Chattopadhyay. 2010. Cholesterol depletion mimics the effect of cytoskeletal destabilization on membrane dynamics of the serotonin1A receptor: a zFCS study. *Biophys. J.* 99:1397–1407.

47. Sah, V. P., T. M. Seasholtz, …, J. H. Brown. 2000. The role of Rho in G protein-coupled receptor signal transduction. *Annu. Rev. Pharmacol. Toxicol.* 40:459–489.

48. Pullikuth, A. K., and A. D. Catling. 2007. Scaffold mediated regulation of MAPK signaling and cytoskeletal dynamics: a perspective. *Cell. Signal.* 19:1621–1632.

49. Chichili, G. R., and W. Rodgers. 2007. Clustering of membrane raft proteins by the actin cytoskeleton. *J. Biol. Chem.* 282:36682–36691.

50. Gaus, K., E. Chklovskaia, …, T. Harder. 2005. Condensation of the plasma membrane at the site of T lymphocyte activation. *J. Cell Biol.* 171:121–131.

51. Liu, A. P., and D. A. Fletcher. 2006. Actin polymerization serves as a membrane domain switch in model lipid bilayers. *Biophys. J.* 91: 4064–4070.

52. Chichili, G. R., and W. Rodgers. 2009. Cytoskeleton-membrane interactions in membrane raft structure. *Cell. Mol. Life Sci.* 66:2319–2328.

53. Godfrey, E. W., and R. C. Schwarte. 2010. Nitric oxide and cyclic GMP regulate early events in agrin signaling in skeletal muscle cells. *Exp. Cell Res.* 316:1935–1945.

54. Pato, C., F. Stetzkowski-Marden, …, J. Cartaud. 2008. Role of lipid rafts in agrin-elicited acetylcholine receptor clustering. *Chem. Biol. Interact.* 175:64–67.